Adsorption (2024) 30:1479–1491
https://doi.org/10.1007/s10450-024-00513-3

Upgrading low-concentration oxygen-bearing coal bed methane by dual-reflux vacuum swing adsorption

Yalou Guo[1,2] · Guoping Hu[3] · Liying Liu[4] · Jian Wang[4] · Paul A. Webley[1] · Gang Kevin Li[2]

Received: 6 May 2024 / Revised: 10 June 2024 / Accepted: 13 June 2024 / Published online: 16 July 2024

Abstract
Fugitive methane (CH_4) is a typical by-product of mining processes, which is commonly known as coal bed methane (CBM) or coal mine gas (CMG). The capture of these CH_4 gases can simultaneously avoid greenhouse gas emissions and provide extra energy benefits. However, the explosion risk of low-concentration CBM (CH_4 molar fraction $\leq 30\%$) requires strictly safe operating protocols to conduct the capture process. Dual reflux vacuum swing adsorption (DR-VSA) is a promising candidate with a vacuum operating condition which can lower the explosion risk and simultaneously reach CH_4 enrichment and O_2 removal targets in product and effluent streams. Herein, a low-concentration oxygen-bearing CBM (20% CH_4, 16% O_2 and 64% N_2) can be upgraded to 69.7 mol% in the product gas while ensuring an effluent concentration of 2.5 mol% by the DR-VSA cycle using ionic liquidic zeolites (ILZ) as the adsorbents. A rigorous safety analysis has been conducted to investigate the explosion risk in the adsorption column and product tank, suggesting that the DR-VSA process is a safe technology for upgrading low-concentration oxygen-bearing methane.

1 Introduction

Coal bed methane (CBM) is a typical unconventional natural gas, which has been regarded as an attractive resource to the energy market in recent decades. High-quality CBM (CH_4 concentration $> 95\%$) is generally extracted from the coal seam and can be used or transported by pipeline after the dehydration process [1]. The sub-quality (CH_4 molar fraction is between 30 and 95%) and low-concentration CBM (CH_4 content $< 30\%$) are generally extracted during the coal mining process from the underground coal mine, also known as coal mining methane (CMM), for safety (avoid methane-related accidents) and environmental reasons (reduce the fugitive methane emissions) [2]. The transportation and utilization of low-concentration CBM (LCCBM) is often restricted or even forbidden in many countries and regions due to its explosion risk. Dilution followed by venting is then the only choice, resulting in significant greenhouse gas emissions [3] and huge waste of energy. When the LCCBM is oxygen-bearing, the relevant safety regulations will be even stricter. The triangular flammability diagram, as shown in Fig. 1, can be used to evaluate the safety of methane/air mixture gases, which is widely used as a reference in studies on oxygen-bearing methane enrichment.

Adsorption-based separation process is a promising method for gas separation and has been extensively studied in the capture of LCCBM. Li et al. [5] reported a proportion pressure swing adsorption (PPSA) using a mixture of activated carbon (AC) and carbon molecular sieves (CMS) as adsorbents to upgrade 20% methane from 80% air. This PPSA process can obtain 30% CH_4 product by modifying the bed length and the mass ratio of AC/CMS, while ensuring that the composition of both product and exhausted gases do not fall into the explosion range. Yang et al. [6] demonstrated a pilot-scale vacuum pressure swing adsorption (VPSA) with a vacuum exhaust step to enrich the dilute ventilation air methane (VAM, CH_4 concentration is 0.2%) up to 1.2% in the product. The introduction of vacuum

✉ Paul A. Webley
paul.webley@monash.edu

✉ Gang Kevin Li
li.g@unimelb.edu.au

1 Department of Chemical & Biological Engineering, Monash University, Clayton, VIC 3800, Australia

2 Department of Chemical Engineering, The University of Melbourne, Parkville, VIC 3010, Australia

3 Key Laboratory of Rare Earths, Ganjiang Innovation Academy, Chinese Academy of Sciences, Ganzhou 341119, Jiangxi, China

4 State Environmental Protection Key Laboratory of Eco-Industry, Northeastern University, Shenyang 100819, China

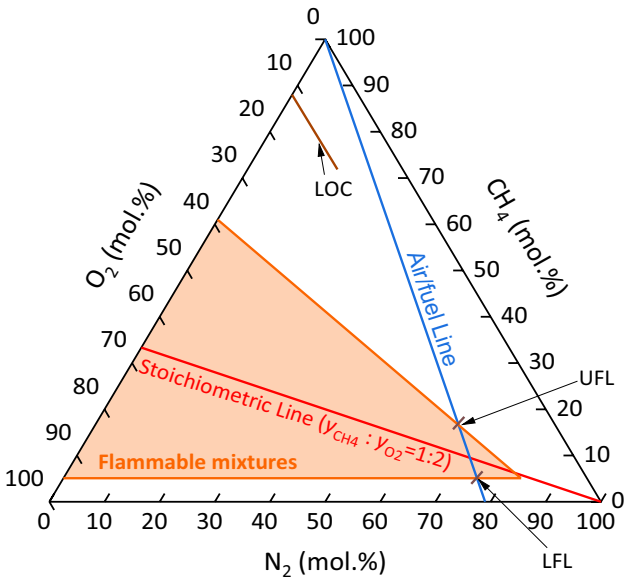

Fig. 1 Methane explosion triangle under normal pressure (101.325 kPa) and temperature (293.15 K). UFL (upper flammability limit in air, 14.9%) and LFL (lower flammability limit in air, 5%) are interactions between two flammable zone boundaries and air/fuel line, and LOC (lowest oxygen concentration for flammability) is 12 mol% [4]

exhaust step can lead to 2–3.45 times increase in the product purity while maintaining the same adsorption/desorption pressure ratio. Bae et al. [7] conducted site trials of a two-stage vacuum, temperature and vacuum swing adsorption (TVSA) process using carbon fiber composites to enrich the VAM (concentration range is 0.54–0.73 vol%) and obtain the final product with a purity of 27.62–35.89 vol%. Qadir et al. used a [$Cu(INA)_2$] metal organic frameworks (MOF) as adsorbents and a 4-bed 6-step VPSA process to enrich 15% oxygen-bearing CH_4 gas up to 50% with a recovery of 90% [8]. Our previous pilot-scale demonstration [9] at a coal mine site shows that a VPSA process using layered adsorption column packed with alumina, activated carbon and ionic liquidic zeolites [10] can be used to separate various CH_4/N_2 mixtures. The feed mixture with CH_4 from 5.6 to 25.1% can be enriched to 27.4–85.5% by introducing a heavy purge step. Yang et al. [11] introduced a CO_2 displacement strategy for regeneration in the adsorption process for the recovery of ventilation air methane, concentrating 10% CH_4 to 89% using activated carbon beads. Qu et al. [12] combined the CO_2-displacement step with VPSA, achieving 75.4% CH_4 purity and 89% recovery from a 10% CH_4 feed gas. Olajossy [13] demonstrated a pilot-scale VPSA with a re-circulated CH_4 rinsing step, which can upgrade raw CMM gas with 53 vol% CH_4 to 96 vol% CH_4. Zhou et al. [2] conducted the performance study and safety analysis of the oxygen-bearing LCCBM enrichment by using a VPSA process in which 25% CH_4 can be enriched to 50.4% with 86.3% recovery. May and co-workers [14–16] developed a lab-scale dual reflux PSA (DR-PSA) apparatus and its corresponding numerical model to investigate the capture of CH_4 (molar fraction between 2.4% and 49.6%) from N_2 gas. Results show that feed gas with 10.4% CH_4 can be enriched to 49.8% in the product and be stripped to 0.7% in the effluent gas. In our previously published work, we introduced a dynamic-feed strategy to solve the so-called mixing problem caused by the lateral feed of DR-PSA, and the new process can achieve a 53.5% CH_4 product from a 2.4% feed gas [17].

From the safety perspective, rising pressure or temperature always results in a wider flammability range, thereby aggravating the explosion risk [18]. Therefore, pressure swing adsorption (PSA) or temperature swing adsorption (TSA) which requires feed gas to be compressed or heated may lead to potential hazards in the enrichment of oxygen-bearing LCCBM. In contrast, vacuum swing adsorption (VSA) operating under vacuum pressure conditions and at ambient temperature can provide a relatively narrower flammable range during the CH_4 enrichment process. Wang et al. [19] demonstrated a kinetic-separation VSA process using CMS to enrich 4.3% CH_4 up to purity of 24.7%. They concluded that the explosion ranges within the adsorption column are narrower during both the adsorption and desorption steps compared with those reported in the previously studied equilibrium-separation VPSA process [2]. N_2 exhibits a weaker interaction with the solid surface compared than CH_4; therefore, common commercial adsorbents, such as activated carbon and zeolites, usually show equilibrium selectivity for CH_4 over N_2 [10, 20–22]. However, some adsorbents show kinetic selectivity for N_2 over CH_4 due to the higher diffusion rate of N_2 than CH_4, such as Engelhard Titanosilicate-4 (ETS-4) [23, 24] and carbon molecular sieve (CMS) [25, 26]. In adsorption, it is more effective to reject the minor components rather than to capture the dominant components from gas mixture. The kinetic process which preferably adsorbs N_2 is more suitable for rejecting N_2 from the CH_4-dominated feed mixture [27, 28], e.g. sub-quality or high-quality CBM gases. For the enrichment of dilute or low-grade CH_4, capturing CH_4 rather than N_2 and O_2 may require less adsorbent loading mass for processing the same amount of feed gas and can be more energy efficient for the VSA process. Thus, it is necessary to develop a CH_4-adsorbing VSA process aimed at the recovery of low-grade CH_4 with great separation performance and a high safety level.

This work aims to investigate the process performance and safety level of a dual-reflux VSA cycle for enriching oxygen-bearing LCCBM using pelletized ionic liquidic zeolites as adsorbents. We examine a case study of a ternary gas mixture consisting of 20% CH_4, 16% O_2 and 64% N_2 on a molar basis, using the DR-VSA process with pressure varying between 0.2 and 1 bar. A detailed safety analysis of external gas circulation

(feed gas and two product gas streams) from initial state to the cyclic steady state (CSS) and internal gas circulation (gas composition along the adsorption column) at different steps when CSS is achieved are conducted based on modified CH_4 explosion triangles under corresponding pressure and temperature conditions.

2 Process modelling

In this study, we have considered the capture of CH_4 from oxygen-bearing LCCBM using a fixed-bed DR-VSA adsorber packed with the pellet ionic liquidic zeolite (ILZ) adsorbent. The LCCBM gas mixture comprises 20 mol% CH_4, 16 mol% O_2 and 64 mol% N_2. We have assumed that the ternary gas mixture is available at normal pressure and temperature. The two primary objectives of this study are enriching the low-grade CH_4 to a purity which meets the safe transportation requirements (restricted to be $\geq 30\%$) and removing the CH_4 content in the effluent gas to guarantee safe emissions (strictly $\leq 2.5\%$).

2.1 Adsorption isotherms

The adsorption isotherms of CH_4, N_2 and O_2 obtained from experiments as well as fitted results based on the Langmuir isotherm equation (Eq. 1) are shown in Fig. 2,

$$q = \frac{q_m \cdot b_0 \cdot p \cdot e^{(-\Delta H/\Re T)}}{1 + b_0 \cdot p \cdot e^{(-\Delta H/\Re T)}} \tag{1}$$

where, q is the gas uptake amount, q_m is the saturated adsorption capacity, b_0 is equilibrium constant, p is the pressure, ΔH is the adsorption enthalpy, $\Re$ is the universal gas constant and T is the temperature.

The pelletized ILZ adsorbents are provided by Gas Capture Technology Pty Ltd. The adsorption isotherms of ILZ are measured using a Micromeritics 3Flex surface characterization setup. The numerical results of the adsorption isotherms are provided in the supplementary information. The Langmuir parameters can be found in Table 1. As shown in Fig. 2, CH_4 is preferably adsorbed (refer to as heavy component) on the ILZ, 5 times that of N_2 and O_2 (refer to as light components) in the vacuum swing pressure window (0.2–1 bar); therefore, CH_4 can be enriched in the heavy gas (product gas) while N_2 and O_2 are collected in the light gas (effluent gas). The excellent selectivity of 5.4 and 5.7 of heavy component (CH_4) against light component (N_2 and O_2, respectively) is determined by Eq. 2 and is also summarized in Table 1,

$$\alpha_{i,j} = \frac{q_i \cdot c_j}{q_j \cdot c_i} \tag{2}$$

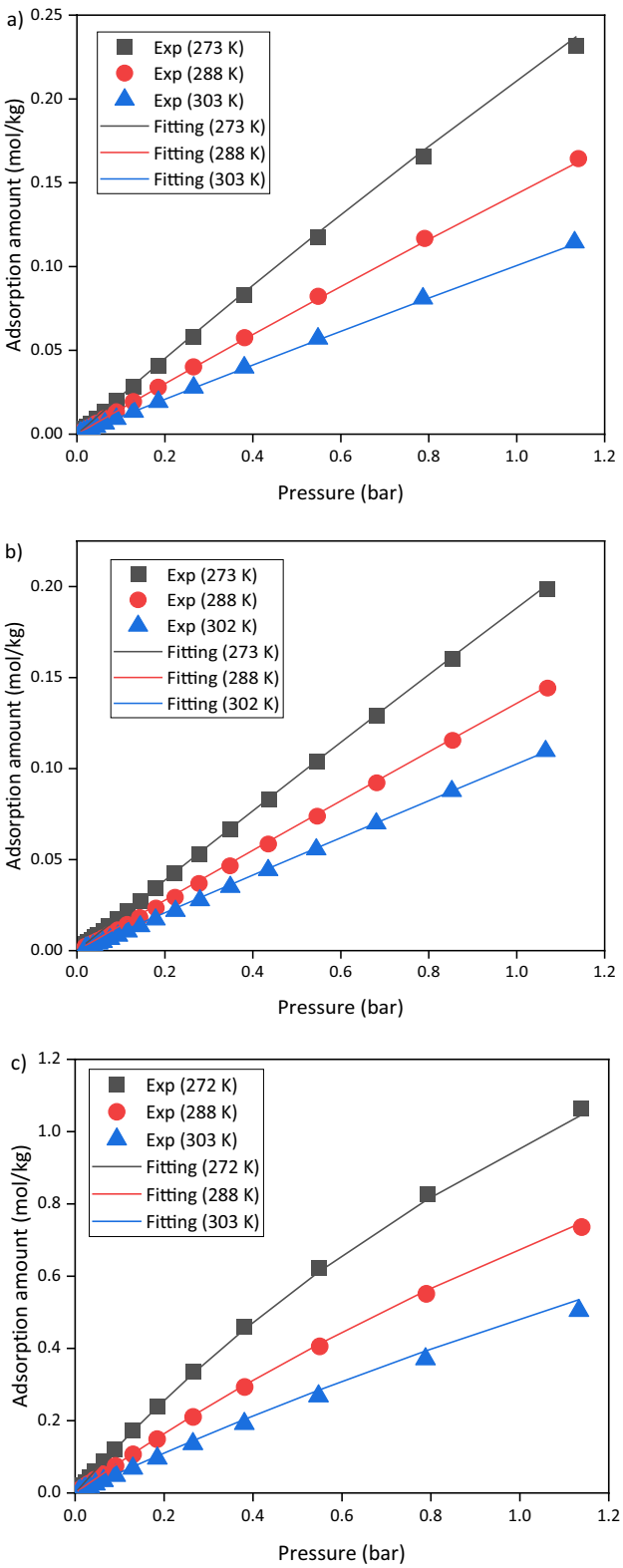

Fig. 2 Adsorption equilibrium isotherms of N_2 (**a**), O_2 (**b**) and CH_4 (**c**) on ILZ

Table 1 Langmuir isotherm fitting parameters and selectivity at 293.15 K

Component	q_m (mol/kg)	b_0 (bar $^{-1}$)	ΔH (kJ/mol)	$\alpha_{CH4,N2}$	$\alpha_{CH4,O2}$
CH_4	3.15	3.66×10^{-5}	21.32	5.38	5.73
N_2	2.54	4.59×10^{-5}	17.19		
O_2	2.72	8.92×10^{-5}	15.25		

where, $\alpha_{i,j}$ denotes the selectivity of component i to component j, q_i and q_j denote the adsorption amount of component i and j and c_i and c_j denote the molar fraction of component i and j in the gas mixture.

2.2 Mathematical model

Several assumptions [16, 29] used to build the numerical model are summarized as follows:

i. Gas-phase properties are described by Peng-Robinson equation.
ii. The mass, velocity and temperature gradients in the bed radial direction are negligible.
iii. The axial pressure drop along bed is calculated using Ergun equation.
iv. The linear driving force (LDF) model with a single lumped mass transfer coefficient is applied.
v. Competitive adsorption behaviors are described by extended Langmuir equation.
vi. Uniform void fraction and adsorbent particles along the bed.

The competitive adsorption between components in gas mixture is described by Extended Langmuir equation, as shown in Eq. 3, using regression parameters calculated by single-component adsorption isotherms,

$$q_i = \frac{q_{m,i}\cdot b_{0,i}\cdot p_i\cdot e^{(-\Delta H_i/\Re T)}}{1+\sum_j b_{0,j}\cdot p_j\cdot e^{(-\Delta H_j/\Re T)}} \tag{3}$$

where q_i is the adsorbed loading of component i, $q_{m,i}$, $b_{0,i}$ and ΔH_i are saturated adsorption amount, equilibrium constant and adsorption enthalpy of component i.

The adsorption column is regarded as one dimension and neglects the radial diffusion of temperature, pressure and concentration in the gas-solid phase. The material balance in the gas phase is described by convection only ignoring the axial dispersion, as shown in Eq. 4,

$$\frac{\partial(v_g c_i)}{\partial z}+[\varepsilon_i+(1-\varepsilon_i)\varepsilon_p]\frac{\partial c_i}{\partial t}+\rho_b\frac{\partial q_i}{\partial t}=0 \tag{4}$$

where, v_g is the superficial gas velocity, z is the axial distance coordinate, ε_i is the bed voidage, ε_p is the particle voidage, ρ_b is the packing density of adsorbent and t is the time.

The momentum balance and pressure drop were calculated by Ergun equation (Eq. 5),

$$\frac{\partial p}{\partial z}=\pm\left(\frac{150\times10^{-5}\mu_g(1-\varepsilon_i)^2}{(2r_p\psi)^2\varepsilon_i^3}v_g+\frac{1.75\times10^{-5}M_W\rho_g(1-\varepsilon_i)}{2r_p\psi\varepsilon_i^3}v_g^2\right) \tag{5}$$

where μ_g is the viscosity of gas mixture, r_p is the particle radius, ψ is the particle shape factor, M_W is the molecular weight of gas mixture and ρ_g is the gas density.

The linear driving force equation (Eq. 6) with constant mass transfer coefficient is used to calculate the flux between gaseous and adsorbed molecules,

$$\frac{\partial q_i}{\partial t}=k_i(q_i^*-q_i) \tag{6}$$

where, k_i is the mass transfer coefficient, q_i is the adsorbed loading in equilibrium with bulk gas of component i.

The energy balance is assumed as non-isothermal. Hence, both gas and solid phase conduction are considered and the heat transfer to the environment is set as rigorous. The governing equation of energy balance can be classified into three parts: solid phase, gas phase and column wall, as described in Eqs. 7–9, respectively,

$$\begin{aligned}&-k_s\frac{\partial^2T_s}{\partial z^2}+C_{ps}\rho_b\frac{\partial T_s}{\partial t}+\rho_b\sum_{i=1}^{n}\left(C_{pai}q_i\right)\frac{\partial T_s}{\partial t}\\&+\rho_b\sum_{i=1}^{n}\left(\Delta H_i\frac{\partial q_i}{\partial t}\right)-h_{gs}a_p(T-T_s)=0\end{aligned} \tag{7}$$

$$\begin{aligned}&-k_g\varepsilon_i\frac{\partial^2T}{\partial z^2}+C_{vg}v_g\rho_g\frac{\partial T}{\partial z}+[\varepsilon_i+(1-\varepsilon_i)\varepsilon_p]C_{vg}\rho_g\frac{\partial T}{\partial t}+p\frac{\partial v_g}{\partial z}\\&+h_{gs}a_p(T-T_S)+\frac{4h_w}{D_B}(T-T_W)=0\end{aligned} \tag{8}$$

$$\begin{aligned}&-k_w\frac{\partial^2T_w}{\partial z^2}+\rho_wC_{pw}\frac{\partial T_w}{\partial t}-h_w\frac{4D_B}{\left(D_B+W_r\right)^2-D_B^2}\left(T-T_w\right)\\&+h_b\frac{4\left(D_B+W_r\right)^2}{\left(D_B+W_r\right)^2-D_B^2}\left(T_w-T_{env}\right)=0\end{aligned} \tag{9}$$

where k_s is the thermal conductivity of the adsorbents, T_s is the temperature of adsorbent, C_{ps} is the specific heat capacity of adsorbent, C_{pai} is the specific heat capacity of the adsorbed gas, h_{gs} is the heat transfer coefficient between gas and solid phase, α_p is the specific particle surface area per unit length of bed, k_g is the heat conductivity of gas phase, C_{vg} is the specific gas phase heat capacity at constant volume, h_w is the heat transfer coefficient between gas and wall, D_B is the internal diameter of column, T_w is the column

wall temperature, k_w is the heat conductivity of wall, ρ_w is the column wall density, C_{pw} is the specific heat capacity of the wall, W_r is the wall thickness, h_b is the heat transfer coefficient between column and ambient and T_{env} is the environmental temperature.

Table 2 Adsorption bed parameters

Parameter	Value	Unit
Column height (H_c)	1	m
Internal diameter (D_B)	0.035	m
Wall thickness (W_r)	0.0016	m
Wall specific heat capacity (C_{pw})	0.5	$kJ{\cdot}kg^{-1}{\cdot}K^{-1}$
Wall-ambient heat transfer coefficient (h_b)	10	$W{\cdot}m^{-2}{\cdot}K^{-1}$
Wall thermal conductivity (k_w)	16	$W{\cdot}m^{-1}{\cdot}K^{-1}$
Inter-particle voidage (ε_p)	0.34	m^3/m^3
Intra-particle voidage (ε_i)	0.36	m^3/m^3
Bulk density (ρ_b)	700	$kg{\cdot}m^3$
Particle radius (r_p)	0.00205	m
Adsorbent specific heat capacity (C_{ps})	0.96	$kJ{\cdot}kg^{-1}{\cdot}K^{-1}$
Adsorbent thermal conductivity (k_s)	0.8	$W{\cdot}m^{-1}{\cdot}K^{-1}$
CH_4 mass transfer coefficient(k_{CH4})	1	s^{-1}
N_2 mass transfer coefficient (k_{N2})	5	s^{-1}
O_2 mass transfer coefficient (k_{O2})	5	s^{-1}

The gas-phase properties are determined using the Peng-Robinson equation (Eq. 10),

$$P = \frac{\mathfrak{R}T}{V_i - b} - \frac{a}{V_i\left(V_i + b\right) + b\left(V_i - b\right)} \tag{10}$$

where a and b are coefficients for Peng-Robinson equation, V_i is the volume of component i, $\mathfrak{R}$ is the universal gas constant.

The mathematical models are built on the Aspen Adsorption platform. Parameters used to construct the DR-VSA model are summarized in Table 2. Each adsorption column is divided into 100 nodes as two separate sections to simulate the lateral feed inlet of DR-VSA cycles. In this research, the dimensionless feed position is constant at 0.5. The governing equations of this model are discretized with Quadratic Upwind Differencing Scheme (QDS) method as partial discretized equations (PDEs), which are solved by implicit Euler iteration with variable step size from 1 to 5 s.

2.3 Process description

The DR-VSA process can be deployed with or without a pressure equalization (PE) step. Figure 3a illustrates a DR-VSA unit without the PE step, which consists of four steps: feed (FE), blowdown (BD), purge (PU) and pressurization

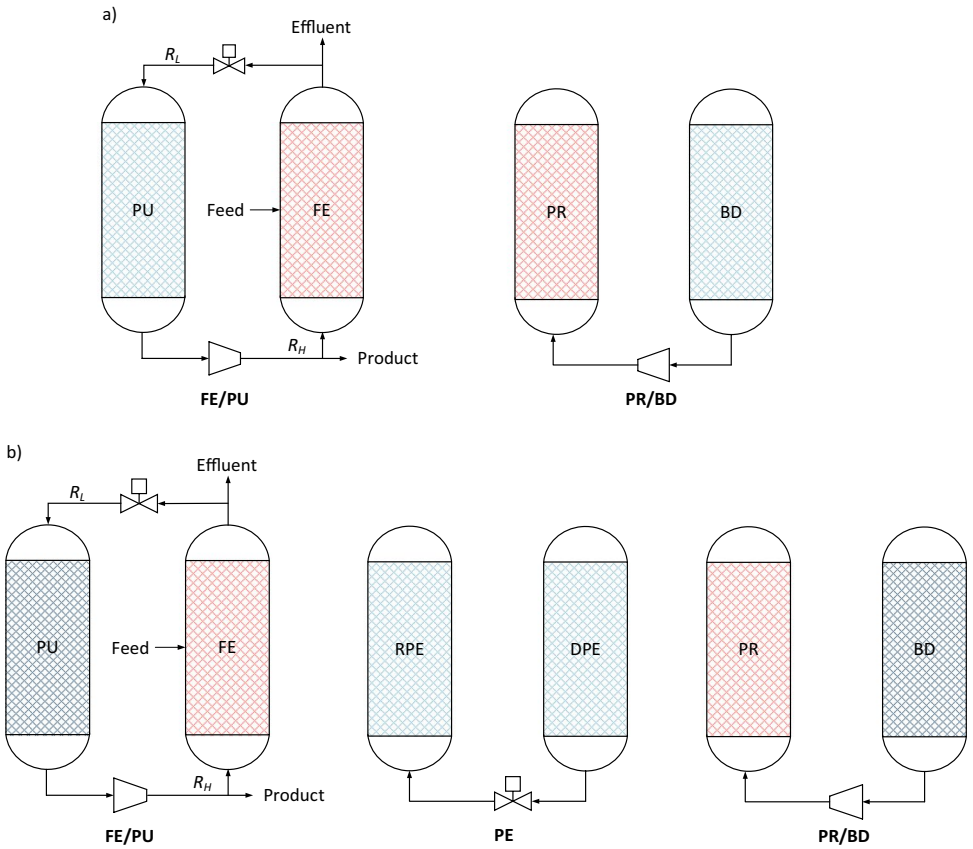

Fig. 3 Schematic diagram of DR-VSA cycle without (**a**) and with (**b**) the pressure equalization (PE) step. R_L: light reflux stream, R_H: heavy reflux stream, FE: feed to high-pressure column, PU: purge in the low-pressure column, RPE: pressure increase during the PE step, DPE: pressure decrease during the PE step, PR: pressurization and BD: blowdown

(PR). The feed gas which is at the atmospheric pressure flows into the high-pressure column (1 bar) at an intermediate position. The two reflux streams comprising mainly heavy or light product are directed to high-pressure column and low-pressure column, respectively. The pressure inversion between two columns is achieved by a vacuum pump at the heavy end. The DR-VSA cycle with PE step is shown in Fig. 3b, containing six steps: FE, DPE (pressure decrease in the PE step), BD, PU, RPE and PR. The major aim of introducing the PE step is to decrease the energy cost of pressure reversal between two adsorption columns. The PE step is simply completed by connecting two columns at the heavy end. The pressure history curves for 6-step DR-VSA cycle at the cyclic steady state (CSS) are presented in (Fig. 4).

2.4 Performance indicators

There are three main performance indicators, i.e., product purity, CH_4 recovery rate, and specific energy consumption, to evaluate the separation results of DR-VSA process and two rigorous CH_4 concentration limits for product ($\geq$30.0 mol%) and effluent gas streams ($\leq$2.5 mol%) according to safety regulations.

The product purity is the average concentration of CH_4 collected from the heavy gas per cycle, which calculated as:

$$y_H = \frac{\int_0^{t_F} \left(c_{H,\mathrm{CH_4}} \cdot H\right) dt}{\sum_{i=1}^{n} \int_0^{t_F} \left(c_{H,i} \cdot H\right) dt} \tag{11}$$

Here, H is the molar flowrate of heavy gas and is constant in each case, $c_{H,i}$ is the transient concentration of component i in the heavy product flow, t_F is the feed step duration.

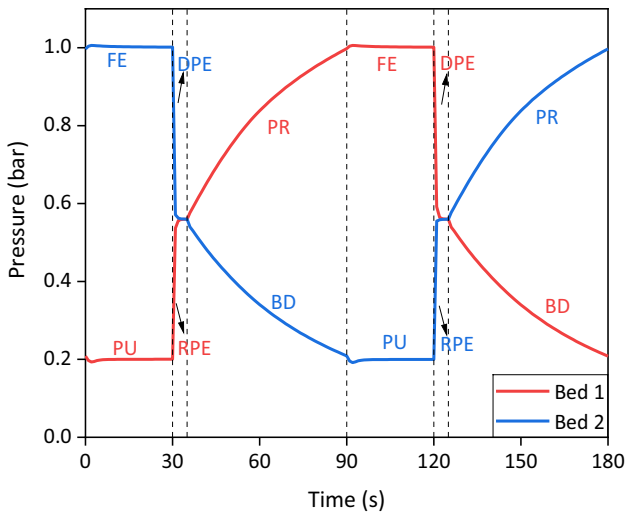

Fig. 4 Bed pressure profiles of 2-bed 6-step DR-VSA cycle

The recovery describes the percentage of captured CH_4 by the DR-VSA system, which is determined by the inlet flow and methane lost in the light gas, as described in the follows,

$$R = \frac{\int_0^{t_F} \left(c_{F,\mathrm{CH_4}} \cdot F - c_{L,\mathrm{CH_4}} \cdot L\right) dt}{\sum_{i=1}^{n} \int_0^{t_F} \left(c_{F,\mathrm{CH_4}} \cdot F\right) dt} \tag{12}$$

where $c_{F,\mathrm{CH4}}$ and $c_{L,\mathrm{CH4}}$ is the transient concentration of methane in the feed (F) and light (L) gas flow, respectively.

The specific energy consumption ($Sp.E$) describes the energy cost for capturing per mole CH_4 in the product gas, as shown in Eq. 13.

$$Sp.E = \frac{\int_0^{t_{cycle}} \left(\dot{N}_{inlet} \cdot \frac{\gamma}{\gamma-1} (\Re T_{in}) \left(\left(\frac{P_{in}}{P_{out}}\right)^{\frac{\gamma}{\gamma-1}} - 1 \right) \right) dt}{1000 \cdot \int_0^{t_F} \left(c_{H,\mathrm{CH_4}} \cdot H\right) dt} \tag{13}$$

Here, t_{cycle} is the cycle duration, $\dot{N}_{inlet}$ is the molar flowrate of gas flowing through the pump, γ is the specific heat ratio of the gas, T_{in} is the temperature of gas before the pump, P_{in} is the pump inlet pressure while P_{out} is the pump outlet pressure.

The separation results of DR-VSA are assessed using our previously reported method, based on a multiplicative assessment score (σ) [30]. In this research, the energy factor has also been considered in the calculation of σ, as shown in Eq. 14,

$$\sigma = \prod_{i=1}^{n} a_i^{w_i} / \prod_{j=1}^{n} a_j^{w_j} = {y_H}^{w_1} \cdot R^{w_2} / (Sp.E/880)^{w_3} \tag{14}$$

where "880" is the heating value of CH_4 (kJ/mol), which is used to regulate the specific energy consumption to generate a dimensionless parameter. Here, purity and recovery are defined as beneficial criteria with separation targets to obtain higher values whereas the $Sp.E$ is the cost criterion which is aimed to achieve low energy duty. As one of the main aims of upgrading low-concentration CH_4 is to produce fuel gases as a supplementary to the energy market, the energy requirement should be a crucial indicator for evaluating the process performance. The optimization can be biased towards enhancing purity or recovery or reducing energy cost by giving more weight in the calculation of σ. Detailed analysis will be included in the following section.

3 Results and discussion

3.1 Effects of pressure equalization step

Pressure equalization step has been well studied and adopted in PVSA [9, 31, 32] for reducing energy consumption and enhancing recovery of light product, particularly for process with high pressure ratio. The DR-PSA processes reported in

open literature usually consists of only four basic steps based on our best knowledge. Herein, a basic comparison between two cycles is conducted to provide some insights on the impact of a PE step on DR-PSA cycles. As shown in Fig. 5, introducing an extra PE step can significantly decrease the energy cost (roughly 40%) with neglectable reduction in the purity and recovery of methane (both < 3%) and oxygen (both < 0.5%) in the range of investigated operating conditions. For separation performance at *H*/*F* ratio of 0.3, introducing the PE step will only result in a slight decrease in the CH_4 purity (66.3% versus 64.5%), CH_4 recovery (99.5% versus 97.3%), O_2 purity (20.1% versus 20.0%) and O_2 recovery (88.7% versus 88.2%), accompanied by a 37% decrease in the specific energy duty for per mole captured CH_4.

At the start of PE or pressure-inversion step, there is a 0.8 bar pressure drop between two columns, leading to a gas stream transferring from the high-pressure column to the low-pressure through the heavy end, which inevitably carries high-concentration CH_4 and imposes a pressure/concentration shock to the adsorbent. For basic 4-step DR-VSA, the concentration shock happens during the pressure variation steps (i.e., the pressurization and blowdown steps) and is buffered by product tank which has a larger volume of 1.5 L than that of the adsorption column (~ 0.95 L). However, the PE step is usually accomplished by simply connecting two adsorption columns through a pipe with limited volume (5 cc in this work), consequently leading to remarkable flow shock which is faster than mass transfer zone, as shown in Fig. S1 in supplementary information. The detailed pressure profiles and column concentration profiles are provided in Appendix B.

3.2 Parametric study

Operating parameters, such as feed step time (t_F) and light reflux flowrate (R_L) also have a significant impact on the separation performance of the DR-VSA process. Since PE step shows negligible penalty to purity and recovery but apparent benefit on reducing energy consumption, we only use cycles with PE step for the following discussions and analysis.

The CH_4 and O_2 molar fraction in heavy and light gas, as a function of t_F, is displayed in Fig. 6. When feed step is 5 s, it is too short for the adsorption front to reach the end of the adsorption column, so the column is not entirely saturated with the CH_4. During the desorption step, the residual N_2 within the bed will limit the CH_4 product purity. The highest CH_4 purity achieved is 84.1% at $t_F = 10$ s, and further extending the feed step time will result in CH_4 breakthrough, leading to an increase in the CH_4 molar fraction in the effluent gas. The O_2 concentration in light gas shows minimal decrease with longer feed time, aligning with the slightly increasing trend of CH_4 molar fraction in light gas.

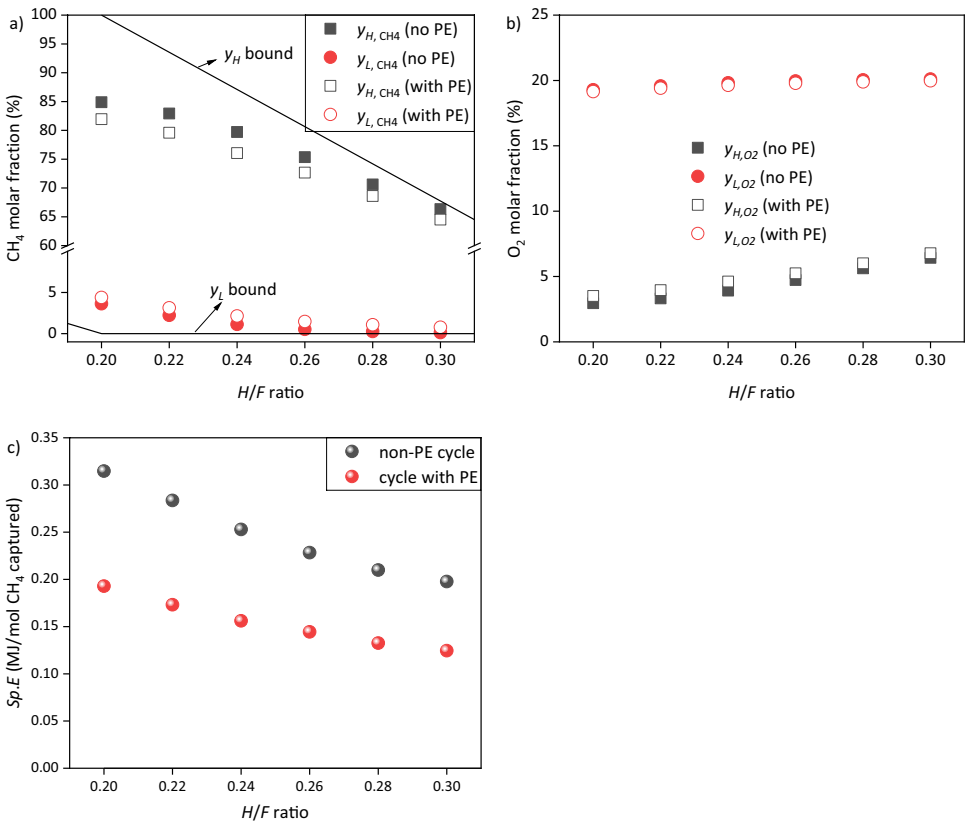

Fig. 5 A comparison of the separation performance in terms of (**a**) CH_4, (**b**) O_2 and (**c**) energy penalty between two DR-VSA processes with and without a PE step as a function of various *H*/*F* ratios ($t_F = 30$ s and $R_L = 1$ slpm)

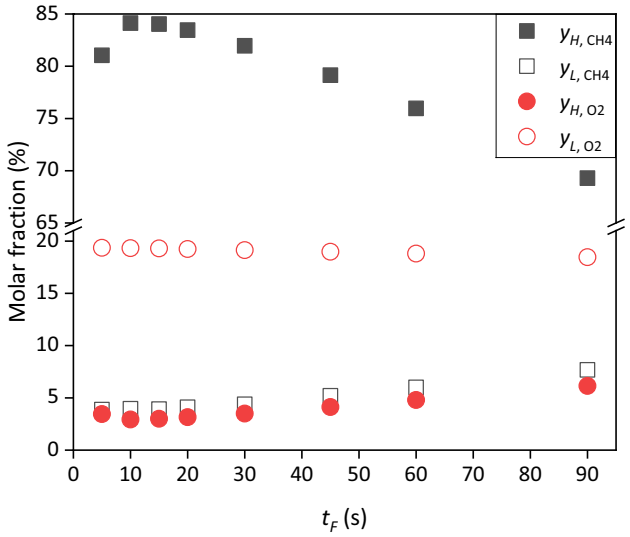

Fig. 6 Effects of feed step time (t_F) on the CH_4 and O_2 molar fraction in heavy (solid) and light (hollow) gases ($H/F = 0.2$ and $R_L = 1$ slpm)

Extending the feed step time also results in more light components passing through the heavy end, as illustrated by the hollow square in Fig. 6, which adversely affects the purity of the CH_4 product.

Figure 7 show effects of R_L on the CH_4 and O_2 content in two outlet gases and specific energy consumption. The optimum R_L value, aimed at increasing the CH_4 concentration in the product gas and reducing its escape, is determined to be 0.75 slpm, as illustrated in Fig. 7a. The R_L exhibits negligible effects on the O_2 concentration in both gas streams. Figure 7b depicts a proportional correlation between specific energy consumption and R_L. It should be noted that when R_L exceeds 0.5 slpm, additional increments only marginally enhance product purity and negligibly reduce fugitive CH_4, while significantly increasing energy penalty. This reveals the importance of integrating energy considerations into the optimization process.

3.3 Optimization

The optimization approach in this study uses the dual-convergence integration algorithm [30] with the modification of three operating parameters, i.e., H/F ratio, feed step duration and light reflux flowrate. The separation performance of each case is evaluated based on the assessment score σ with three indicators (KPIs): product purity, CH_4 recovery and energy duty. The introduction of assessment score (σ) can dramatically improve the optimization efficiency. However, giving the weight of three KPIs is arbitrary and challenging due to the extensively reported trade-offs between different indicators, especially the trade-off between purity and recovery. These weights have significant impacts on the optimization of DR-VSA cycle. Various optimal results based on different weights for three KPIs are summarized in Table 3 to provide a basic understanding about how σ affects the final optimal results. The numbers in the first column indicate weight of purity, recovery and specific energy consumption, respectively. The second column shows the

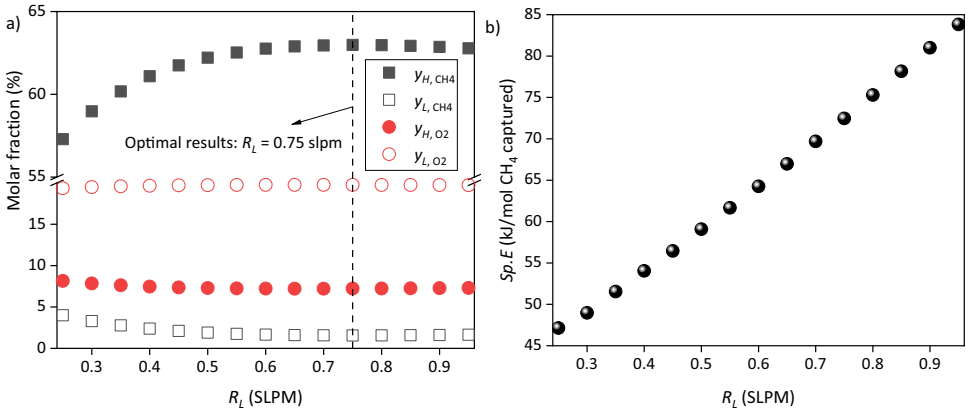

Fig. 7 Effects of light reflux flowrate (R_L) on the separation performance: **a** CH_4 and O_2 molar fraction in heavy and light gases; and (**b**) specific energy consumption for per mole captured CH_4 (($H/F = 0.3$ and $t_F = 65$ s)

Table 3 Determination of optimal separation performance under different assessment scores (σ)

No.	Weight of KPIs	Operating parameters	y_H (%)	R (%)	Sp.E (kJ/mol CH_4)
1	[0.5, 0.5, 0]	[0.21, 10 s, 1.50 slpm]	83.9	90.0	474.4
2	[0.45, 0.45, 0.1]	[0.26, 55 s, 0.60 slpm]	69.7	90.6	79.9
3	[0.4, 0.5, 0.1]	[0.28, 60 s, 0.55 slpm]	65.9	92.2	68.0
4	[0.4, 0.4, 0.2]	[0.37, 135 s, 0.30 slpm]	49.9	92.2	27.8

optimal operating conditions with the sequence of *H*/*F* ratio, feed step time and light reflux flowrate.

As shown in Table 3, the optimization can be biased towards targeting any higher results of these three indicators. For case 1, separation process is adjusted to obtain high purity and recovery without consideration of energy duty. Although satisfactory purity (83.9%) and recovery (90.0%) is achieved, the extremely high energy demand (474.4 kJ/mol CH_4 captured) leave neglectable energy benefits for the captured CH_4. In contrast, the energy duty can be lowered to 27.8 kJ for per mole captured CH_4 when its weight is elevated to 0.2 whilst CH_4 purity declines to 49.4%. All separation results and corresponding operational conditions relevant to this section are summarized in Appendix A.

The detailed optimization route of case 2 is shown in Fig. 8. The optimized separation performance is 69.7% CH_4 purity with 90.6% recovery and the specific energy consumption of 79.9 kJ per mole captured CH_4 under the following operational parameters: $H/F = 0.26$, t_F=55 s and R_L=0.60 slpm. The following safety analysis is conducted using the column's profiles and results collected from boundary streams in this case.

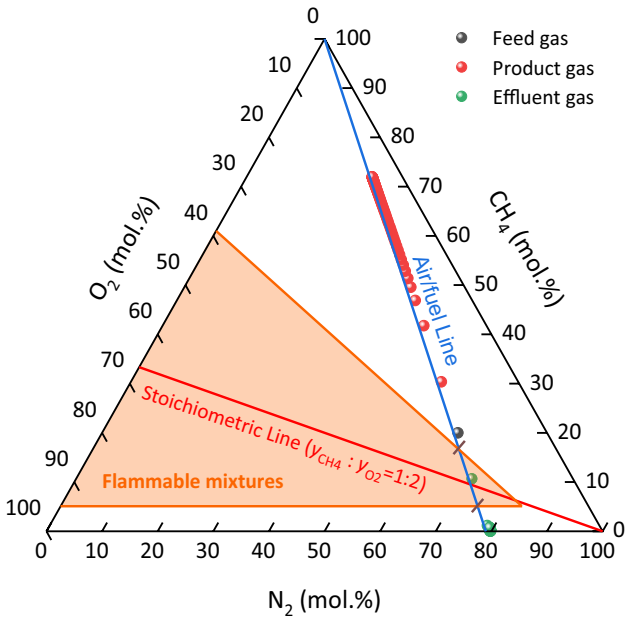

Fig. 9 Safety analysis of gas tank with methane explosion triangle under normal pressure and temperature (NPT). Black dot indicates the feed gas composition. Red and green dots represent compositions in the product and effluent gas tank after each cycle, respectively

3.4 Safety analysis

Methane explosion triangle is usually used to evaluate the possibility of flammable gas mixtures [1, 4, 33, 34]. As shown in Fig. 9, the black dot indicates the feed gas with a constant composition whereas the red and green dots represent compositions in the product and effluent gas tank, respectively, and each dot shows the gas composition after each cycle. The feed gas is assumed as a mixture of CH_4 and air, and the ratio of nitrogen and oxygen is equal to that of the air. All of these results are located close to the so-called "air/fuel line" due to the similar adsorption properties of nitrogen and oxygen on the ILZ adsorbent. This analysis is from the initial run to the operation at the cyclic steady state (CSS). As shown in Fig. 9, there is one green dot falling into the explosive range, which represents the composition in the effluent gas tank after the first cycle with a duration only lasting for approximately 3 min. Once the system reaches the CSS, the feed, product and effluent gas are always out of the explosion range, indicating that there is no explosion risk.

The safety analysis of adsorption columns is more challenging due to its dynamic nature during a single cycle. The pressure, temperature and composition profiles as well as the corresponding calculated UFL, LFL and LOC at each position during a cycle under CCS are summarized in the Appendix B. The flammable zone is determined where CH_4 concentration falls between range of UFL and LFL while O_2 concentration is higher than the LOC. Herein, we only depict the widest flammable zone of each step, as shown in Fig. 10. During the purge step, the CH_4-dilute gas flows

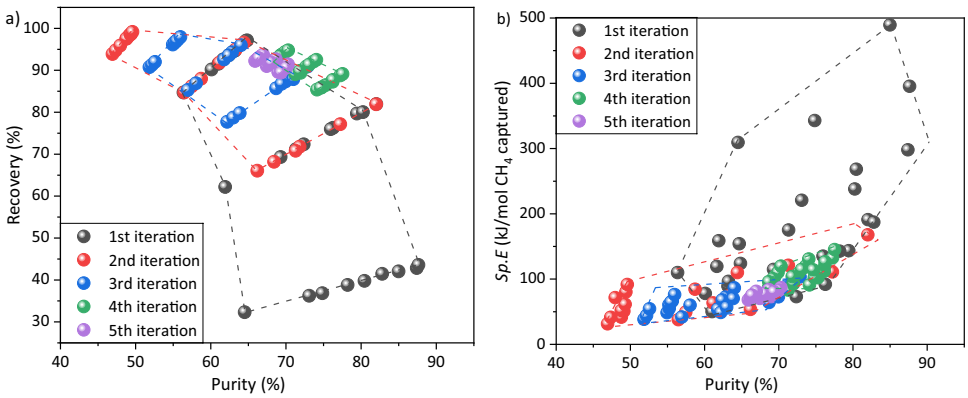

Fig. 8 Optimization of DR-VSA process for 20% CH_4 gas enrichment: **a** purity versus recovery and (**b**) purity versus specific energy consumption

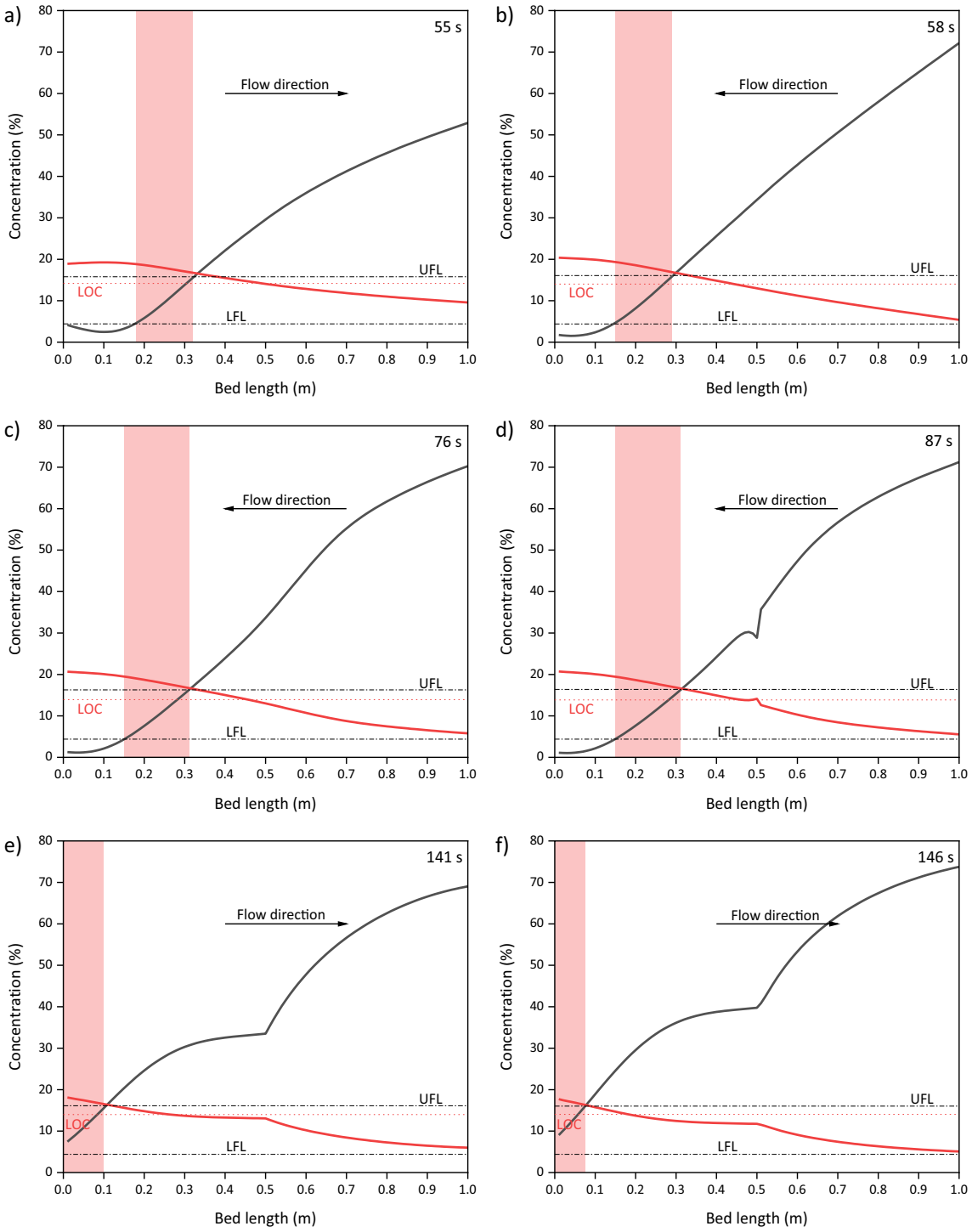

Fig. 10 Gas concentration of CH_4 (black) and O_2 (red) and the widest explosive risk range (highlighted in red strip) within the column at PU (a), RPE (b), PR (c), FE (d), DPE (e) and BD (f) step

from the light end to the heavy end while explosive range expands during this step. The widest flammable zone, as indicated in Fig. 10a, happens at the end of this step (55 s) when the explosive range located between Z of 0.18–0.32 m, accounts roughly 15% of the total adsorption column. Gas flow direction is reversed during the following RPE and pressurization steps. Due to the remarkable concentration shock during the RPE step, the flammable zone firstly moves to the light end at start and then back forward to the heavy end. At 58 s (the 3 s of the PER step), the explosion zone takes

Table 4 Comparison of results from this work and other reported studies

case	CH_4 in feed [mol%]	O_2 bearing	CH_4 purity [mol%]	CH_4 recovery [%]	Sp.E (kJ/mol CH_4)	Process	Source
1	25	√	50.4%	86.3%	*66.9	PVSA	[2]
2	20	√	69.7%	90.6%	79.9	DR-VSA	This work
3	10.4	×	42.4%	93%	235	DR-PSA	[15]
4	2.4	×	51.3%	34%	1544	DR-PSA	[15]
5	4.3	√	24.7%	86%	~400	VSA	[19]

*This value is transformed from kWh·Nm^{-3} feed based on its original value, feed CH_4 concentration and CH_4 recovery reported in the reference

up 15% of the whole bed (Fig. 10b). The flammable zone remains stable (accounts around 16% of the column) during the pressurization step. The screenshot at 76 s, i.e., the 16 s of the PR step, was selected to be exhibited in Fig. 10c. During the feed step, the flammable zone moves forward the light end and starts to shrink since 130 s. The widest flammable zone of FE, DPE and BD step is determined at 87, 141 and 146 s of the whole cycle and takes up 17%, 10% and 7% of the column, respectively, as shown in Fig. 10d-f. At the end of BD step, there is no explosion zone within the column at all. The column safety analysis validates the high safety level of this DR-PSA process for enriching 20% CH_4 and air mixture. The widest flammable zone (17% of the whole column during feed step) in this research is comparable to what is reported in the kinetic-separation VSA process (21% of the total bed length during adsorption) [19] and much shorter than that determined in the equilibrium-separation VPSA cycles (nearly 75% at the start of the pressurization step) [2].

3.5 Comparison with reported work

A comparison with other processes for low-grade CH_4 capture reported in the literature is summarized in Table 4. The specific energy consumption is found to be deeply associated with the feed concentration as more gases are needed to be processed for per mole captured CH_4 and the corresponding working capacity of adsorbents is small when feed concentration is low. The most like-for-like case to this work is case 1 in Table 4 which employs a PVSA step to enrich 25% CH_4 feed gas [2]. This DR-VSA process can deliver better CH_4 purity and recovery with comparable energy duty while ensuring a much narrower flammable zone within the column at the CSS. DR-VSA also requires lower power duty (~ 10 kJ) than DR-PSA (~ 20 kJ) from the perspective of processing per mole feed gas due to its lower requirement of reflux flowrate [15]. According to the reported studies [14, 15], the optimal R_L typically ranges between 2 and 4 slpm for DR-PSA cycles to provide adequate gas to push the adsorption/purge front forward close to the heavy/light end. However, this value is often lower than 1 slpm for DR-VSA cycles.

4 Conclusions

In this work, a DR-VSA process for capture methane from oxygen-bearing LCCBM was numerically investigated with a comprehensive safety analysis. Simulation results show that the 6-step DR-PSA process can enrich the CH_4 up to 69.7% in the product gas with a recovery of 90.6% from feed gas consisting of 20% CH_4 and 80% air. The column history profiles at the CSS and composition of boundary gases from initial run to the CSS are collected to determine the flammable zone within the bed and evaluate the safety level of product tanks. The tank safety analysis determines an extremely short period (3 min) when flammability is possible in the light product tank during the operation from start-up to steady run, suggesting high safety level from the perspective of system boundary. The column safety analysis shows that the explosion zone in the adsorption bed of this equilibrium-separation DR-VSA is comparable to that of the kinetic-separation VSA and much smaller than that of the PVSA in both feed (adsorption) and purge (desorption) steps.

Supplementary Information The online version contains supplementary material available at https://doi.org/10.1007/s10450-024-00513-3.

Acknowledgements Y. Guo would like to thank his wife, Ms. Xuewei Gu, and his newborn son, Yijia Alexander Guo, for all the love, support, and joy they have brought to his life.

Author contributions All authors contributed to the study conception and design. Yalou Guo: Conceptualization; formal analysis; investigation; visualization; writing – original draft; writing – review and editing. Guoping Hu: Software; visualization; writing – review and editing. Liying Liu: Data curation; resources; investigation. Jian Wang: Data curation; resources. Paul A. Webley: Supervision; formal analysis; funding acquisition; writing –review and editing. Gang Kevin Li: Conceptualization; funding acquisition; supervision; writing – review and editing. All authors read and approved the final manuscript.

Funding Open Access funding enabled and organized by CAUL and its Member Institutions. This work is sponsored by the Australia Research Council (DP19010133). G. Hu acknowledges the financial support by the Self-deployed Project of Ganjiang Innovation Academy, Chinese Academy of Sciences, the Double Thousand Plan of Jiangxi Province (jxsq2023101060), and the Bureau of Science and Technology, Taiyuan, entitled 'the enrichment of coal bed methane using novel

adsorbents via pressure swing adsorption'. L. Liu is grateful to the support by National Natural Science Foundation of China (Grant No. 22078054).

Data availability Data is provided within the manuscript or supplementary information files.

Declarations

Ethics approval It is not applicable.

Consent to participate It is not applicable.

Consent for publication It is not applicable.

Competing interests The authors declare no competing interests.

References

1. Zhao, P., et al.: A review of oxygen removal from oxygen-bearing coal-mine methane. Environ. Sci. Pollut Res. Int. **24**(18), 15240–15253 (2017)
2. Zhou, Y., et al.: Upgrade of low-concentration oxygen-bearing coal bed methane by a vacuum pressure swing adsorption process: Performance study and safety analysis. Energy Fuels. **30**(2), 1496–1509 (2016)
3. Su, S., Agnew, J.: Catalytic combustion of coal mine ventilation air methane. Fuel. **85**(9), 1201–1210 (2006)
4. Mashuga, C.V., Crowl, D.A.: Application of the flammability diagram for evaluation of fire and explosion hazards of flammable vapors. Process Saf. Prog. **17**(3), 176–183 (1998)
5. Li, Y.L., Liu, Y.S., Yang, X.: Proportion pressure swing adsorption for low concentration coal mine methane enrichment. Sep. Sci. Technol. **48**(8), 1201–1210 (2013)
6. Yang, X., et al.: Vacuum exhaust process in pilot-scale vacuum pressure swing adsorption for coal mine ventilation air methane enrichment. Energies **11**(5), 1030–1042 (2018)
7. Bae, J.-S., et al.: Site trials of ventilation air methane enrichment with two-stage vacuum, temperature, and vacuum swing adsorption. Ind. Eng. Chem. Res. **59**(35), 15732–15741 (2020)
8. Qadir, S., et al.: Experimental and numerical investigations on the separation performance of [Cu(INA)2] adsorbent for CH4 recovery by VPSA from oxygen-bearing coal mine methane. Chem. Eng. J. **408**, 127238–127250 (2021)
9. Hu, G., et al.: Separation of methane and nitrogen using heavy reflux pressure swing adsorption: Experiments and modeling. Ind. Eng. Chem. Res. **62**(18), 7114–7126 (2023)
10. Li, G., et al.: Method for gas separation. US Patent, US20170348670A1 (2015)
11. Yang, Y., et al.: Enrichment of ventilation air methane by adsorption with displacement chromatography technology: Experiment and numerical simulation. Chem. Eng. Sci. **149**, 215–228 (2016)
12. Qu, D., et al.: Enrichment of low-grade methane gas from nitrogen mixture by VPSA with CO2 displacement process: Modeling and experiment. Chem. Eng. J. **380**, 122509–122522 (2020)
13. Olajossy, A.: Effective recovery of methane from coal mine methane gas by vacuum pressure swing adsorption: A pilot scale case study. Chem. Eng. Sci. **1**(4), 46–54 (2013)
14. May, E.F., et al.: Demonstration and optimisation of the four dual-reflux pressure swing adsorption configurations. Sep. Purif. Technol. **177**, 161–175 (2017)
15. Saleman, T.L., et al.: Capture of low grade methane from nitrogen gas using dual-reflux pressure swing adsorption. Chem. Eng. J. **281**, 739–748 (2015)
16. Zhang, Y.C., et al.: Non-isothermal numerical simulations of dual reflux pressure swing adsorption cycles for separating N2 + CH4. Chem. Eng. J. **292**, 366–381 (2016)
17. Guo, Y., et al.: Capture of dilute methane with a novel dynamic-feed dual-reflux pressure swing adsorption process. AIChE J. **68**(1), e17390 (2021)
18. Vanderstraeten, B., et al.: Experimental study of the pressure and temperature dependence on the upper flammability limit of methane/air mixtures. J. Hazard. Mater. **56**(3), 237–246 (1997)
19. Wang, X., et al.: Kinetic-separation vacuum swing adsorption for safe and efficient enrichment of low concentration coal mine gas. Sep. Purif. Technol. **299**, 121683–121697 (2022)
20. Hofman, P.S., et al.: A dynamic column breakthrough apparatus for adsorption capacity measurements with quantitative uncertainties. Adsorption. **18**(3–4), 251–263 (2012)
21. Bastos-Neto, M., et al.: Adsorption measurements of nitrogen and methane in hydrogen-rich mixtures at high pressures. Ind. Eng. Chem. Res. **50**(17), 10211–10221 (2011)
22. Xiao, G., et al.: Adsorption equilibria and kinetics of CH4 and N2 on commercial zeolites and carbons. Adsorption. **23**(1), 131–147 (2016)
23. Butwell, K.F., Dolan, W.B., Kuznicki, S.M.: Selective removal of nitrogen from natural gas by pressure swing adsorption. US Patent, US6197092B1 (2001)
24. Butwell, K.F., Dolan, W.B., Kuznicki, S.M.: Selective removal of nitrogen from natural gas by pressure swing adsorption. US Patent, US6315817B1 (2001)
25. Cavenati, S., Grande, C., Rodrigues, A.: Separation of methane and nitrogen by adsorption on carbon molecular sieve. Sep. Sci. Technol. **40**(13), 2721–2743 (2005)
26. Yang, X., et al.: Practical separation performance evaluation of coal mine methane upgrading with carbon molecular sieves. Chem. Eng. J. **367**, 295–303 (2019)
27. Effendy, S., Xu, C., Farooq, S.: Optimization of a pressure swing adsorption process for nitrogen rejection from natural gas. Ind. Eng. Chem. Res. **56**(18), 5417–5431 (2017)
28. Xiao, G., et al.: Nitrogen rejection from methane using dual-reflux pressure swing adsorption with a kinetically-selective adsorbent. Chem. Eng. J. **372**, 1038–1046 (2019)
29. Da Silva, F.A., Silva, J.A., Rodrigues, A.E.: A general package for the simulation of cyclic adsorption processes. Adsorpt.-J. Int. Adsorpt. Soc. **5**(3), 229–244 (1999)

30. Guo, Y., et al.: Enrichment of low-grade methane by dual reflux vacuum swing adsorption. Sep. Purif. Technol. **301**, 121907–121919 (2022)
31. Yavary, M., Ebrahim, H.A., Falamaki, C.: The effect of number of pressure equalization steps on the performance of pressure swing adsorption process. Chem. Eng. Process. **87**, 35–44 (2015)
32. Hu, G., et al.: Separation of methane and nitrogen using ionic liquidic zeolites by pressure vacuum swing adsorption. AIChE J. **68**(7), e17668 (2022)
33. Li, Y.L., et al.: A novel VPSA process for ventilation air methane enrichment by active carbon. Adv. Mater. Res. **479**, 648–653 (2012)
34. Yang, X., et al.: Safe Separation of the Low-Concentration and Oxygen-Bearing Coal Mine Methane by Vacuum Pressure Swing Adsorption. Adsorpt. Sci. Technol. **32**(8), 667–679 (2014)